Vol.4, No.3, Page 1871- 1880, 2026 https://doi.org/10.59628/jast.v4i3.2636 ISSN 2958-9568 JAST

SUN PUBLISHER

مجلة جامعة صنعاء للعلوم التطبيقية والتكنولوجيا

Sana'a University Journal of Applied Sciences and Technology

https://journals.su.edu.ye/index.php/jast/

Synthesis, Spectroscopic Characterization, and Antibacterial Evaluation of Novel Organophosphorus Schiff Base Derivatives Derived from Chlorodiphenylphosphine

Dheya A. Hameed [1], Fathi M. Al-Azab[1], Yasmin M.S. Jamil[1], Nedhal A.A. Al-Selwi [1*] and Gamil M.S. Qasem[1,2]

[1]**Department of Chemistry, Faculty of Sciences, Sana'a University, Sana'a, Yemen,**
[2]**Department of Chemistry, Faculty of Applied Sciences, Thamar University, Thamar, Yemen**

*Corresponding author: n.alsalwi@su.edu.ye

Abstract

In this study, three novel organophosphorus Schiff base derivatives (OPC_1–OPC_3) were successfully synthesized by condensing chlorodiphenylphosphine with different Schiff bases derived from various aldehydes and hydrazine derivatives. The structural elucidation of the synthesized compounds was achieved using comprehensive spectroscopic analyses, including FTIR, UV-Vis, and both ^{1}H and ^{13}C-NMR spectroscopy. Elemental analysis and physical property measurements further confirmed the proposed molecular structures. Spectroscopic data revealed characteristic azomethine (C=N), phosphorus–carbon (P–C), and phosphorus–oxygen (P–O–C) stretching bands, confirming the successful formation of the organophosphorus Schiff base framework. The synthesized compounds were tested for antibacterial activity against *Escherichia coli*, *Pseudomonas aeruginosa*, and *Staphylococcus aureus* using the agar well diffusion method. The results demonstrated that all compounds exhibited moderate to significant antibacterial activity, with OPC_2 and OPC_3 showing notable inhibition zones compared to OPC_1. These findings suggest that the incorporation of organophosphorus moieties into Schiff base ligands enhances their biological potency and provides a promising route for developing new bioactive organophosphorus materials.

Article Info

Keywords:
Organophosphorus compounds, Spectral studies, Antibacterial Study, Schaff bases

Article History:
Received: 15-December-2025,
Revised: 22-January-2026,
Accepted: 10-February -2026,
Published: 28 March 2026.

1. INTRODUCTION

Schiff bases represent one of the most versatile classes of organic compounds, characterized by the azomethine (–C=N–) functional group formed through the condensation of primary amines with aldehydes or ketones [1, 2] . Since their discovery by Hugo Schiff in 1864, these compounds have attracted extensive attention owing to their wide range of applications in coordination chemistry, catalysis, analytical chemistry, and medicinal research [3, 4]. The azomethine linkage plays a crucial role in stabilizing transition metal ions through coordination, thereby enhancing the chemical and biological reactivity of the resulting complexes [5, 6].

The structural diversity and ease of modification of Schiff bases allow for the fine-tuning of their physicochemical and biological properties. Schiff base ligands incorporating heteroatoms, such as oxygen, nitrogen, sulfur, and phosphorus, exhibit enhanced chelating ability and bioactivity [7] . In particular, the incorporation of organophosphorus moieties into Schiff base frameworks introduces additional donor sites, improving lipophilicity and cellular permeability, which can lead to improved antimicrobial, antitumor, and enzymatic inhibition properties [8–10]. Organophosphorus derivatives have therefore emerged as promising scaffolds for the design of biologically active compounds and functional materials [11].

Recent investigations have focused on the synthesis of Schiff base–derived metal complexes and organophosphorus derivatives because of their notable pharmacological properties, such as antibacterial [12], antifungal [13], antimalarial [14], anti-inflammatory, anti-HIV, and anticancer activities [15]. Moreover, the versatility of these compounds extends to industrial and environmental applications, including catalysis, corrosion inhibition, and polymer stabilization [16, 17]. Their rich coordination chemistry enables the design of complexes with tailored electronic and structural characteristics suitable for advanced functional materials.

Previous studies by our group and other researchers have demonstrated that Schiff base ligands bearing organophosphorus functionalities can form stable complexes with transition metals, displaying significant antimicrobial potential and structural diversity [11–14]. However, the synthesis and comprehensive characterization of new organophosphorus Schiff bases, particularly those incorporating hydrazone, semicarbazone, or thiosemicarbazone moieties, remain largely unexplored.

In this study, we report the synthesis and full spectroscopic characterization of three novel organophosphorus Schiff base (OP) compounds (OPC_1–OPC_3) obtained by condensing chlorodiphenylphosphine with different azomethine compounds. The resulting derivatives were characterized using FTIR, UV–Vis, ^{1}H NMR, ^{13}C NMR, and elemental analysis. Furthermore, their antibacterial activities were evaluated against *Staphylococcus aureus*, *Escherichia coli*, *and Pseudomonas aeruginosa* using the agar well diffusion method. The results highlight the influence of structural variations and phosphorus substitution on the biological efficacy of these newly synthesized compounds, thereby contributing to the ongoing search for potent organophosphorus-based antibacterial agents.

2. MATERIALS AND METHODS

2.1. Materials

Reagent-grade chemicals, such as chlorodiphenylphosphine (Riedel de Haën), triethylamine (Riedel de Haën), thiosemicarbamide (BDH), ethylenediamine (Riedel de Haën), phenylhydrazine (BDH), and orthohydroxybenzaldehyde (BDH), were utilized in this investigation without any purification. The solvents used were of spectroscopic grade.

2.2. Preparation of organophosphorus Schiff base

Solutions of the appropriate Schiff bases (SB_1(0.02 mol), SB_2 (0.02 mol), and SB_3 (0.02 mol)) in dry acetonitrile were treated with triethylamine, followed by the dropwise addition of chlorodiphenylphosphine (0.04 mol) with SB_1, (0.02 mol) with SB_2, and SB_3 under stirring. The reaction mixture was refluxed for 2 h after the complete addition. After filtering the solid (triethylamine hydrochloride), the solvent was evaporated, and the product was washed with cold ethanol and recrystallized to afford the corresponding organophosphorus derivatives, OPC_1, OPC_2, and OPC_3, as solid products (Scheme 1).

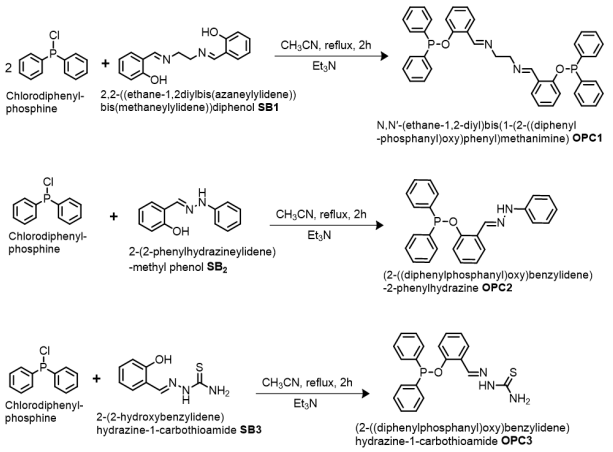

Scheme 1: Synthesis of Organophosphorus compounds (OPC_1, OPC_2, and OPC_3)

2.3. Physical and Spectral Measurements

An FT/IR-140 (Jasco, Japan) apparatus at Sana'a University was used to measure the infrared spectra of the compounds in the 200–4000 cm $-$ 1 range. At Sana'a University, the electronic spectra of the compounds were measured in the 200–800 nm range using a UV-VIS spectrophotometer (Specord200, Analytik Jena, Germany). The proton NMR spectra were obtained at 25°C, 850 and 213 MHz using a Bruker spectrometer. Elemental analyses (C, H, and N) were performed at the Central Laboratory, Faculty of Science, Cairo University, Egypt, using Vario EL Fab. CHN Nr. 11042023. Stuart Scientific electrothermal melting point instrument was used to test the melting points of the compounds in glass capillary tubes in °C.

2.4. Biological Screening

The antibacterial properties of the synthesized compounds were tested against *Escherichia coli*, *Pseudomonas aeruginosa*, and *Staphylococcus aureus*. Antibacterial activity was assessed using the agar well diffusion method [18]. Stock solutions with a concentration of 1000 μg/mL were produced using DMSO as a solvent. Various concentrations of 100, 200, and 300 μg/mL were then prepared using these solutions. Bacteria invaded the surface of the nutrient agar. Various concentrations of the chemicals were added to the wells and ditches

Table 1. Physical properties and Elemental Analysis of the synthesized Organophosphorus compounds

Compounds	Color (Yield%)	M.P (°C)	F. Wt. (g/mole)	Element Analysis Calculated% (Found%)				
				C	H	N	P	S
OPC_1	Yellow (55)	157	636.67	52.89 (52.77)	2.47 (2.41)	11.04 (11.00)	9.18 (9.10)	–
OPC_2	Green (75)	106	396.43	61.42 (61.36)	5.55 (5.50)	14.55 (14.48)	7.47 (7.44)	–
OPC_3	White (82)	183	379.42	62.09 (62.01)	5.45 (5.37)	16.87 (16.81)	10.22 (10.17)	8.44 (8.00)

created on the agar plates. Gentamicin (120 μg/mL) was used as the reference material. Each Petri dish was incubated for 24 h at 37°C. The results were recorded by calculating the diameter of the inhibition zone (mm).

3. RESULTS AND DISCUSSION

The organophosphorus compounds OPC_1, OPC_2, and OPC_3 were produced by condensing chlorodiphenylphosphine with 2,2-((ethane-1,2-diylbis(azaneylylidene))bis(methaneylylidene))diphenol SB_1 2:1, 4-(N,N-dimethylaminobenzaldehyde) SB_2 1:1, 2-(2-phenylhydrazineylidene)methyl phenol, and 2-(2-hydroxybenzylidene)hydrazine-1-carbothioamide SB_3 1:1, respectively. All the synthesized compounds are stable, have bright colors, and can be stored at room temperature for long periods. The compounds are soluble in common organic solvents, such as ethanol, DMF, and DMSO, but are insoluble in water. Table 1 lists the physical and analytical characteristics of some of the compounds.

3.1. NMR Spectra

3.1.1. ^{1}H NMR spectrum of OPC_1

The ^{1}H NMR spectrum of OPC_1 (in DMSO-d_6, Figure 1) exhibits a set of multiplet signals in the range of δ7.01–8.18 ppm, corresponding to the aromatic protons of the phenyl rings. A distinct singlet observed at δ 9.68 ppm (s, 1H) is assigned to the azomethine proton (–CH=N–), confirming the successful formation of the Schiff base linkage [14, 19]. The –CH_2– protons of OPC_1 appear at δ 3.08 ppm [20]. The integration values and proton assignments are consistent with the proposed molecular structure and follow standard spectroscopic reporting conventions.

3.1.2. ^{13}C NMR spectrum of OPC_1

The ^{13}C NMR spectrum of OPC_1 recorded in DMSO-d_6 (Figure 2) shows a characteristic signal at δ 132.93 ppm [14], attributed to the azomethine carbon (C=N). Multiple resonances observed between δ 128.52 and 132.93 ppm are assigned to aromatic carbon atoms [21] [24]. A signal at approximately δ 40. ppm is assigned to the residual DMSO-d_6 solvent and has been explicitly identified as such to avoid misinterpretation.

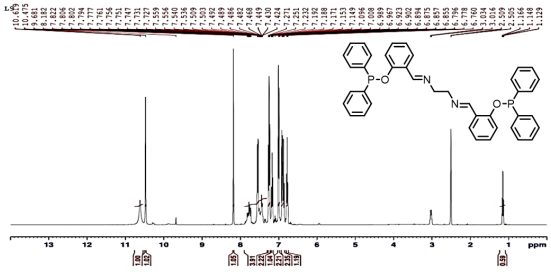

Figure 1. ^{1}H NMR spectrum of the OPC_1

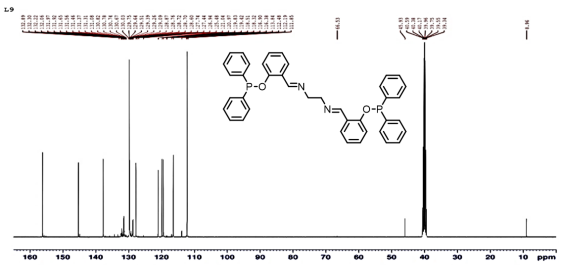

Figure 2. ^{13}C NMR spectrum of the OPC_1

3.1.3. ^{1}H NMR spectrum of OPC_2

The ^{1}H NMR spectrum of OPC_2 (in DMSO-d_6, Figure 3) displays aromatic proton signals as multiplets in the range of δ7.26–7.96 ppm, corresponding to the phenyl and substituted aromatic rings. The azomethine proton (–CH=N–) appears as a singlet at δ 8.71 ppm (s, 1H) [19]. In addition, a weak singlet at δ 10.22 ppm (s, 1H) is assigned to the imine –NH proton [22]. All signals are reported with appropriate chemical shifts, multiplicities, integrations, and assignments, ensuring consistency with standard ^{1}H NMR reporting.

3.1.4. ^{13}C NMR spectrum of OPC_2

The ^{13}C NMR spectrum of OPC_2 in DMSO-d_6 (Figure 4 4) shows a downfield resonance at δ 157.41 ppm [23], which is attributed to the azomethine carbon (C=N). Aromatic carbon signals are observed in the range of δ 111.85–145.89 ppm [24]. The methylene carbon (–CH_2–) appears as a weak signal at δ 66.32 ppm. A signal

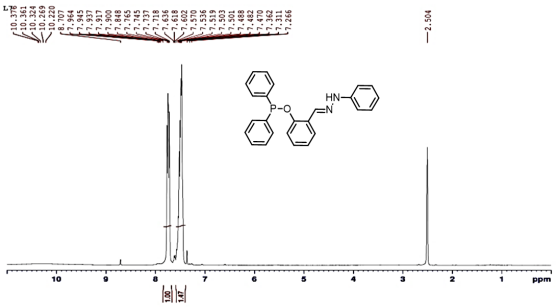

Figure 3. ^{1}H NMR spectrum of the OPC_2

at approximately δ 40. ppm is assigned to the residual DMSO-d_6 solvent and has been explicitly identified as such to avoid misinterpretation.

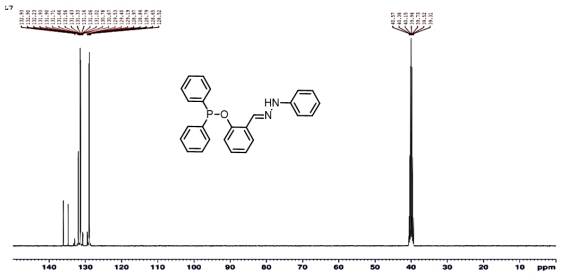

Figure 4. ^{13}C NMR spectrum of the OPC_2

3.1.5. ^{1}H NMR spectrum of OPC_3

The ^{1}H NMR spectrum of OPC_3 (in DMSO-d_6, Figure 5) exhibits multiplet signals between δ 6.79 and 8.37 ppm, corresponding to aromatic protons. The azomethine proton (–CH=N–) appears as a singlet at δ 9.82 ppm (s, 1H) [19]. The signal at δ 11.68 ppm (s, 1H) is attributed to the –NH proton, whereas the signal at δ 3.38 ppm (br s, 2H) is assigned to the –NH_2 group [22] .

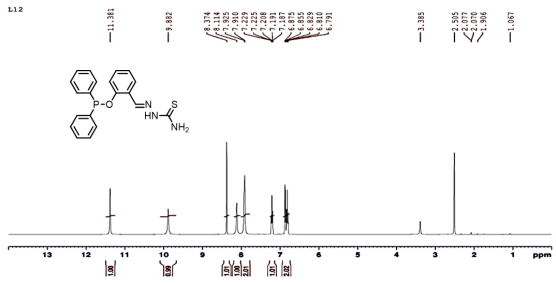

Figure 5. ^{1}H NMR spectrum of the OPC_3

3.1.6. ^{13}C NMR spectrum of OPC_3

The ^{13}C NMR spectrum of OPC_3 recorded in DMSO-d_6 (Figure 6) shows a resonance at δ 178.07 ppm, attributed to the thiocarbonyl carbon (C=S), and a signal at δ 156.86 ppm, corresponding to the azomethine carbon (C=N) [25]. Aromatic carbon resonances are observed in the range δ 116.49–140.06 ppm [23]. A signal detected at approximately δ 40 ppm is assigned to the residual DMSO-d_6 solvent and has been explicitly identified as such to avoid misinterpretation. The observed carbon signals are consistent with the proposed structure of OPC_3, considering the overlap and symmetry effects.

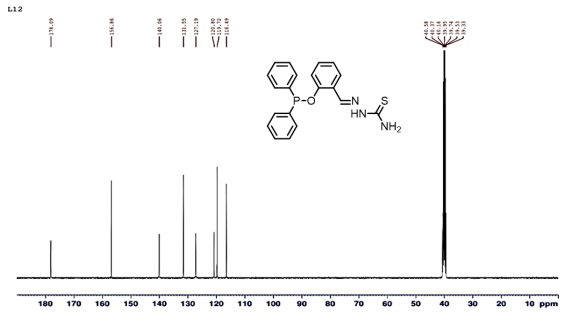

Figure 6. ^{13}C NMR spectrum of the OPC_3

3.2. FTIR spectra Studies

3.2.1. IR spectrum of OPC_1

The FT-IR spectrum of SB_1 (Figure 7) is characterized by a strong azomethine stretching vibration, υ(C=N), observed in the region of 1610–1620 cm^{-1}, confirming the formation of the Schiff base framework. The broad absorptions in the 3200–3500 cm^{-1} region are attributed to phenolic υ(O–H) stretching, while the aromatic υ(C–H) and υ(C=C) vibrations appear near 3050–3100 cm^{-1} and 1500–1580 cm^{-1}, respectively [20].

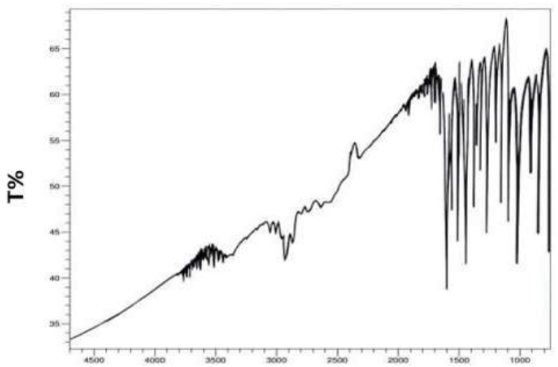

Figure 7. IR spectrum of the SB_1

Upon conversion to OPC_1 (Figure 8), the υ(C=N) band is retained but appears at 1605 cm^{-1} [26], showing a slight downward shift relative to SB_1. This shift indicates a redistribution of electron density around the azomethine linkage due to the introduction of the organophosphorus moiety. A key diagnostic difference is the disappearance of the phenolic υ(O–H) band, consistent with its involvement in P–O bond formation.

Most importantly, new absorption bands appear in the

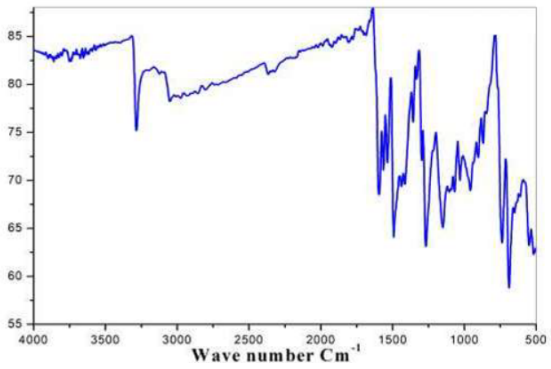

Figure 8. IR spectrum of the OPC_1

OPC_1 spectrum at 1170 and 1078 cm $^{-1}$, assigned to υ(P–C) and υ(P–O–C) stretching vibrations, respectively [27]. These bands are completely absent in SB_1 and provide unambiguous evidence for successful phosphination. The aromatic υ(C–H) stretching at 3078 cm $^{-1}$ and υ(C=C) stretching at 1545 cm $^{-1}$ are preserved in both spectra, confirming that the aromatic framework remains intact.

3.2.2. IR spectrum of OPC_2

The IR spectrum of SB_2 (Figure 9) exhibits a characteristic azomethine υ(C=N) band near 1615–1625 cm^{-1}, together with an N–H stretching vibration in the 3300–3350 cm^{-1}, region, consistent with its hydrazone structure. Aromatic υ(C–H) and υ(C=C) vibrations are observed near 3080 cm^{-1}, and 1540–1560 cm^{-1}, respectively.

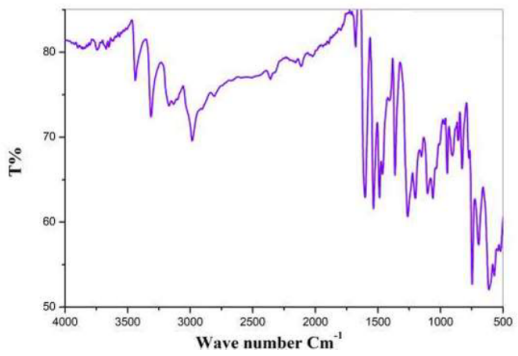

Figure 9. IR spectrum of the SB_2

In OPC_2 (Figure 10), the azomethine ν(C=N) band persists at 1611 cm $^{-1}$, confirming that the Schiff base skeleton is preserved after reaction with chlorodiphenylphosphine. The slight shift relative to SB_2 reflects the electronic perturbation induced by the phosphorus substituent. The N–H stretching band remains visible at 3314 cm $^{-1}$, indicating that this functional group is not directly involved in the P–N bond formation.

New P-specific bands appear exclusively in OPC_2 at

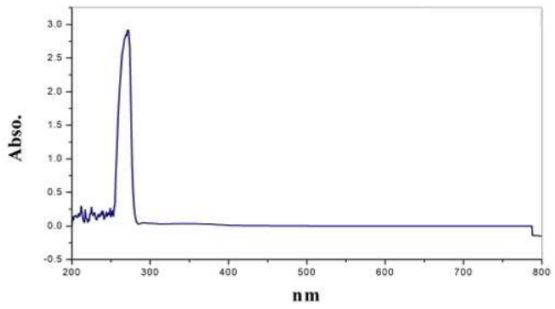

Figure 10. IR spectrum of the OPC_2

1188 and 1072 cm $^{-1}$ (ν(P–C) and ν(P–O–C), respectively) [26, 28]. These absorptions are absent in SB_2 and represent the most diagnostic spectral evidence for OP incorporation. Aromatic ν(C–H) stretching at 3082 cm $^{-1}$ and ν(C=C) stretching at 1540 cm $^{-1}$ remain essentially unchanged, demonstrating that phosphination does not disrupt the aromatic system.

3.2.3. IR spectrum of OPC_3

The FT-IR spectrum of SB_3 (Figure 11) shows a strong azomethine ν(C=N) band in the 1620–1640 cm $^{-1}$ region, accompanied by a characteristic thiocarbonyl ν(C=S) vibration at approximately 1250–1270 cm $^{-1}$1, confirming the presence of the thiosemicarbazone moiety. Broad absorptions in the 3200–3400 cm $^{-1}$1 region are assigned to $\nu(NH/NH_2)$ stretching vibrations, while aromatic ν(C–H) bands appear near 3100 cm $^{-1}$.

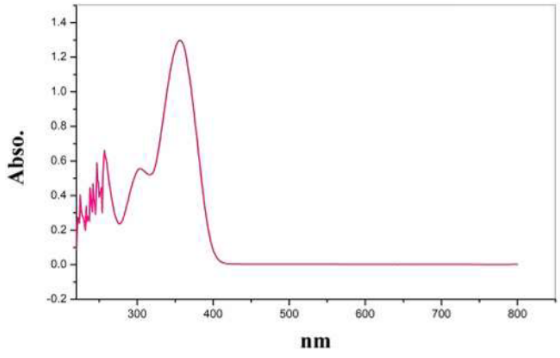

Figure 11. IR spectrum of the SB_3

In OPC_3 (Figure 12), both key functional groups are retained: the azomethine ν(C=N) band appears at 1645 cm $^{-1}$, and the thiocarbonyl ν(C=S) band is observed at 1255 cm $^{-1}$ [29]. The persistence of these bands confirms that phosphination occurs without disrupting the hydrazone–thioamide framework. Minor shifts in band positions relative to SB_3 reflect changes in conjugation and electron density caused by phosphorus substitution. New absorption bands at 1172 and 1038 cm $^{-1}$ are observed exclusively in OPC_3 and are assigned to the P–C (ν(P–C)) and P–O–C (ν(P–O–C)) stretching vibrations, respectively [26]. These bands are absent in SB_3 and

Table 2. The IR absorption bands of the OPC_s

Compound	ν(C=N)	ν(P-O-C)	ν(C=C)	ν(C-H)	ν(C=S)	ν(P-C)	ν(NH-NH_2)
OPC_1	1605	1078	1545	3078	–	1170	–
OPC_2	1611	1072	1540	3082	–	1188	3314
OPC_3	1645	1038	1644	3100	1255	1172	3244

serve as definitive markers of organophosphorus incorporation. The aromatic ν(C–H) stretching at 3100 cm $^{-1}$ and ν(C=C) vibrations near 1645 cm $^{-1}$ remain

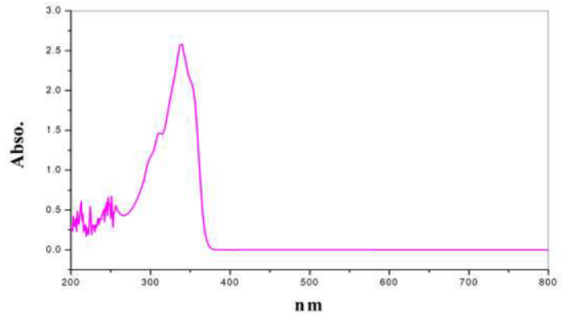

Figure 12. IR spectrum of the OPC_3

The characteristic FTIR absorption bands of the synthesized compounds are summarized in Table 2, supporting the vibrational assignments and structural confirmation.

The comparative FTIR spectra of OPC_1–OPC_3 are shown in Figure 13, which illustrates the characteristic absorption bands corresponding to P–C, P–O–C, and C=N vibrations.

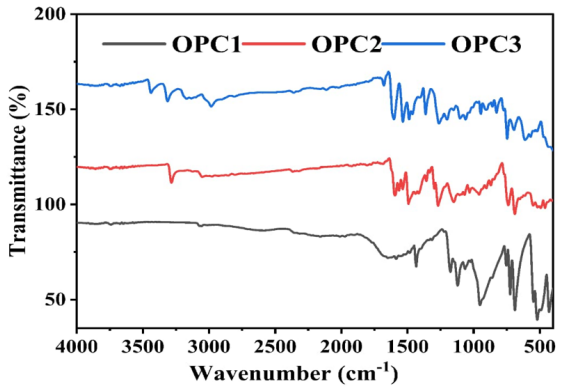

Figure 13. IR spectra of OPC_1, OPC_2, and OPC_3

3.3. Electronic spectra

3.3.1. *Electronic spectrum OPC_1*

The OPC_1 UV-vis spectrum in the region of 200–800 nm (Figure 14) was recorded in a DMSO solution. The n-π* transition is linked to bands at 257–285 nm in Figure 10, which may be connected to OPC_1 (yellow). Nonbonding electrons on the nitrogen of the electronic absorption bands undergo an n-π* transition to a lower energy [14].

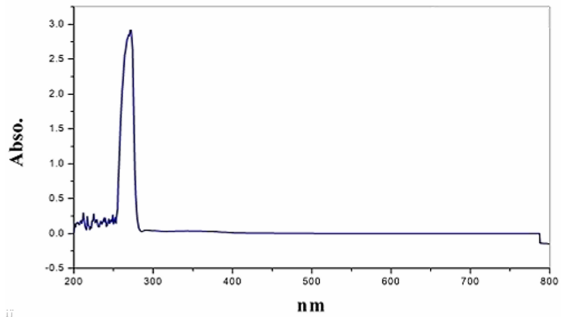

Figure 14. UV–visible spectrum of the OPC_1

3.3.2. *Electronic spectrum OPC_2*

OPC_2, which is green, may be connected to the absorbance bands at 312 and 359 nm in the ligand UV-Vis spectrum (Figure 15). Bands at approximately 310–355 nm are linked to the n-π* transition. Additionally, Figure 11 designates bands in the 300–360 nm range. Bands observed between 270 and 310 nm are categorized as π-π* transitions [29]. The electronic absorption bands shift to lower energies owing to the n-π* transition of the nonbonding electrons on the nitrogen of the azomethine group in the organophosphorus Schiff base [22].

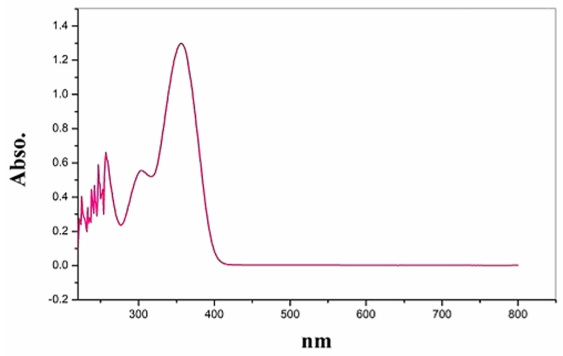

Figure 15. UV–visible spectrum of the OPC_2

3.3.3. *Electronic spectrum OPC_3*

The absorbance bands at 360 and 310 nm, respectively, in the compound UV-Vis spectrum (Figure 16) may be

attributed to OPC_3 (White) and indicate the n-π^* and π-π^* transitions in the OPC_3 aromatic rings. Unlike OPC_3, the electronic absorption bands in OPC_3 shift to lower energy due to the n-π^* transition of the nonbonding electrons on the nitrogen of the azomethine group [29]. The combined UV-Vis spectra of OPC_1–OPC_3 are shown in Figure 17.

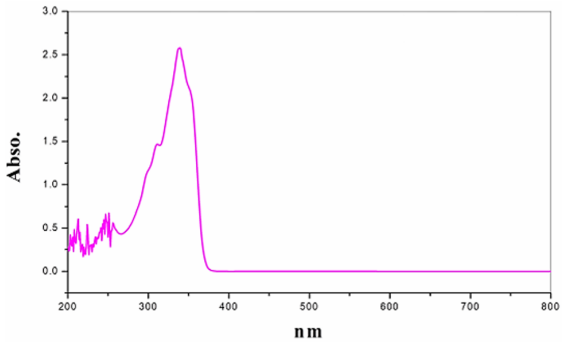

Figure 16. UV–visible spectrum of the OPC_3

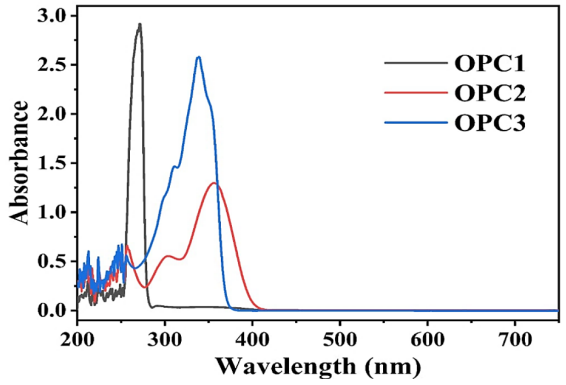

Figure 17. UV–visible spectra of the OPC_1 – OPC_3

3.4. Antibacterial Study

The synthesized organophosphorus Schiff base derivatives (OPC_1–OPC_3) exhibited clear antibacterial activity against *Staphylococcus aureus*, *Escherichia coli*, and *Pseudomonas aeruginosa*, with inhibition zones increasing proportionally with concentration (Table 3 3) (Figures **??**). This dose-dependent pattern is consistent with the typical antimicrobial behavior of Schiff bases and organophosphorus derivatives, reflecting direct molecular interactions with bacterial targets rather than passive diffusion effects [12, 30].

The enhanced activities observed for OPC_2 and OPC_3 relative to OPC_1 can be attributed to their structural characteristics. The azomethine (–C=N–) group is widely recognized as the pharmacophoric site in Schiff bases, which are capable of coordinating with biological macromolecules and interfering with enzymatic activity. Furthermore, the incorporation of phosphorus donor moieties (P–C, P–O–C) improves molecular lipophilicity, thereby facilitating penetration through bacterial membranes. Several studies have confirmed that Schiff bases enriched with heteroatoms, such as N, O, S, and P, exhibit superior biological functions owing to improved electron delocalization and target-binding capability [11, 12, 31].

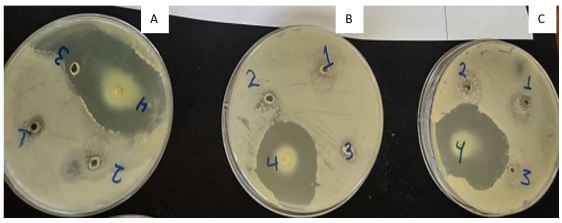

Figure 18. Inhibition zone of OPC_1 with different bacterial strains: *Escherichia coli* (A), *Pseudomonas aeruginosa* (B), and *Staphylococcus aureus* (C), using different concentrations 100 μg/mL (1), 200 μg/mL (2), 300 μg/mL (3), and Gentamicin 300 μg/mL (4) as a standard.

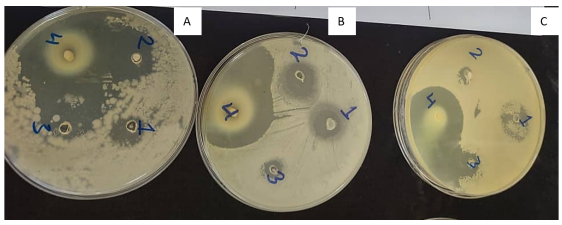

Figure 19. Inhibition zone of OPC_2 with different bacterial strains: *Escherichia coli* (A), *Pseudomonas aeruginosa* (B), and *Staphylococcus aureus* (C), using different concentrations 100 μg/mL (1), 200 μg/mL (2), 300 μg/mL (3), and Gentamicin 300 μg/mL (4) as a standard.

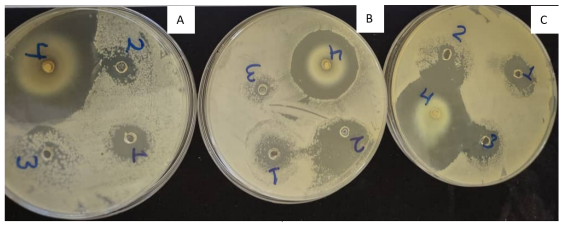

Figure 20. Inhibition zone of OPC_3 with different bacterial strains: *Escherichia coli* (A), *Pseudomonas aeruginosa* (B), and *Staphylococcus aureus* (C), using different concentrations 100 μg/mL (1), 200 μg/mL (2), 300 μg/mL (3), and Gentamicin 300 μg/mL (4) as a standard.

OPC_3 produced the strongest antibacterial response among the synthesized compounds, particularly against *E. coli* and *P. aeruginosa*. This enhanced efficacy can be attributed to the presence of thioamide (C=S) and hydrazone groups, which increase nucleophilicity and facilitate stronger coordination or hydrogen-bond inter-

Table 3. Antibacterial effect of the synthesized OPC compounds.

Compound	Concentration	Zone of inhibition in mm		
	μg/ml	*Staphylococcus aureus*	*Pseudomonas aeruginosa*	*Escherichia coli*
	100	6	8	12
OPC_1	200	10	10	15
	300	11	12	16
Gentamicin	300	25	28	30
	100	12	10	14
OPC_2	200	14	12	20
	300	16	15	22
Gentamicin	300	24	22	28
	100	10	8	12
OPC_3	200	14	12	14
	300	15	15	18
Gentamicin	300	26	24	28

actions with bacterial proteins. Similar enhancements have been reported for thiosemicarbazone- and sulfur-containing Schiff bases, wherein sulfur-rich sites foster stronger interactions with microbial enzymes and disrupt cellular respiration and DNA synthesis [32].

The relatively lower antibacterial activity of OPC_1 can be rationalized by its simpler bis-phenolic framework, which lacks additional donor functionalities. The reduced ability for electron delocalization and target coordination limits its interaction with bacterial components. Comparable findings have been reported for phenolic Schiff bases lacking sulfur or additional heteroatom substituents, which generally show weaker antimicrobial effects [11, 33].

Variations in the susceptibility of gram-positive and gram-negative bacteria can be attributed to their different cell-wall architectures. Gram-negative bacterial membranes possess a lipopolysaccharide-rich outer layer that restricts the entry of many antimicrobial agents. However, OPC_2 and OPC_3 demonstrated notable activity against *E. coli* and *P. aeruginosa*, indicating strong lipophilicity and effective membrane diffusion. Similar trends have been reported for organophosphorus and hydrazone-based Schiff bases, in which increased hydrophobicity enhances interactions with gram-negative lipid bilayers [13, 34].

Overall, the antibacterial performance of the synthesized organophosphorus Schiff base derivatives aligns with well-established mechanisms, including metal chelation, inhibition of bacterial enzymes, destabilization of cell membranes, and interference with cellular respiration [22, 26, 35]. The pronounced bioactivity of OPC_2 and OPC_3 underscores the value of phosphorus, sulfur, and hydrazone functionalities in augmenting antibacterial potency. Furthermore, extensive literature indicates that further coordination with transition metals could significantly enhance their redox properties, membrane permeability, and target affinity, suggesting that these ligands are promising scaffolds for the development of next-generation antimicrobial agents [11, 14].

4. CONCLUSION

This study successfully developed and characterized three novel organophosphorus Schiff base derivatives (OPC_1–OPC_3) via the reaction of chlorodiphenylphosphine with different azomethines. Combined spectroscopic (FTIR, UV-Vis, and NMR) and elemental analyses confirmed the proposed molecular structures and the coordination of phosphorus through P–C and P–O–C linkages. The synthesized compounds exhibited thermal stability, distinct coloration, and solubility in organic solvents. Biological screening results revealed notable antibacterial activities, particularly for OPC_2 and OPC_3, which demonstrated strong inhibition against both gram-positive and gram-negative bacteria. This study highlights the potential of organophosphorus Schiff bases as promising candidates for antibacterial applications and encourages further investigation into their metal complexation and pharmacological properties.

REFERENCES

[1] S. Bhandarkar, P. Pathare, and B. Khobragade, "New nickel (ii), copper (ii) and cobalt (ii) complexes based salicylaldehyde schiff base: Synthesis, characterisation, and antiviral activity," *Mater. Today: Proc.*, vol. 92, pp. 807–816, 2023.

[2] J. Zhao and G. Cui, "Study on adsorption and complexation behavior of thiourea on copper surface," *Int. J. Electrochem. Sci.*, vol. 6, no. 9, pp. 4048–4058, 2011. DOI: 10.1016/s1452-3981(23)18309-x.

[3] A. Allouch, I. E. Hassan, and M. Bouchkara, "Synthesis and characterization of complexes of some transition metals

with two bifunctional thiourea derivatives," *Chem. Sci. Trans.*, 2018. DOI: 10.7598/cst2018.1476.

[4] A. Abu-Yamin, M. S. Abduh, S. A. M. Saghir, and N. S. Al-Gabri, "Synthesis, characterization and biological activities of new schiff base compound and its lanthanide complexes," *Pharmaceuticals*, vol. 15, p. 454, 2022. DOI: 10.3390/ph15040454.

[5] H. H. Afridi et al., "Synthesis and investigation of the analgesic potential of enantiomerically pure schiff bases: A mechanistic approach," *Molecules*, vol. 27, no. 16, p. 5206, 2022. DOI: 10.3390/molecules27165206.

[6] K. Hsiu-Ming, K. Wan-Ping, L. Gene-Hsiang, and K. L. Chung, "Mesogenic heterocycles derived from quinoxaline schiff bases," *Tetrahedron*, vol. 72, no. 41, 2016. DOI: 10.1016/j.tet.2016.07.076.

[7] O. A. El-Gammal, F. S. Mohamed, G. N. Rezk, and A. A. El-Bindary, "Structural characterization and biological activity of a new metal complexes based of schiff base," *J. Mol. Liq.*, vol. 330, p. 115 522, 2021.

[8] N. Filipovic, A. Smith, and B. Johnson, "Biological activity of two isomeric n-heteroaromatic selenosemicarbazones and their metal complexes," *Monatshefte fur Chemie - Chem. Mon.*, vol. 145, pp. 1089–1099, 2014. DOI: 10.1007/s00706-014-1197-6.

[9] S. Borhade, "Synthesis, structure, spectroscopy and antimicrobial activity of copper (ii) complex of furfuraldehyde-2-salisaldehyde thiosemicarbazide," *J. Recent Trends Sci. Technol.*, vol. 10, no. 3, pp. 423–429, 2014, Available online.

[10] S. V. Upadhyay, R. V. Zala, and K. D. Bhatt, "Synthesis, characterization and biological screening of schiff bases derived from 4,6-difluoro-2-amino benzothiazole," *Med. & Anal. Chem. Int. J.*, vol. 4, no. 1, pp. 1–7, 2020. DOI: 10.23880/macij-16000157.

[11] Y. M. Jamil, F. M. Al-Azab, N. A. Al-Selwi, T. Alorini, and A. N. Alhakimi, "Preparation, physicochemical characterization, molecular docking and biological activity of a novel schiff-base and organophosphorus schiff base with some transition metal (ii) ions," *Main Group Chem.*, vol. 22, no. 3, pp. 337–362, 2023. DOI: 10.3233/MGC-220101.

[12] F. M. Al-Azab et al., "Titanium complex with new schiff base 4-(n,n-dimethylaminobenzylidene)-1-phenylsemicarbazide: Synthesis, thermal, xrd, and antibacterial properties," *Sana'a Univ. J. Appl. Sci. Technol.*, vol. 2, no. 4, pp. 391–402, 2024.

[13] Y. M. Jamil, F. M. Al-Azab, and N. A. Al-Selwi, "Novel organophosphorus schiff base ligands: Synthesis, characterization, ligational aspects, xrd and biological activity studies," *Ecletica Quimica*, vol. 48, no. 3, pp. 36–53, 2023. DOI: 10.26850/1678-4618eqj.v48.3.2023.p36-53.

[14] Y. M. Jamil, A. Al-Azab, F. M. Al-Azab, and N. A. Al-Selwi, "Larvicidal effects of new organophosphorus schiff base compounds against dengue fever vector aedes aegypti (diptera: Culicidae)," *Sana'a Univ. J. Appl. Sci. Technol.*, vol. 1, no. 1, pp. 78–87, 2023. DOI: 10.59628/jast.v1i1.156.

[15] A. Kamali, R. Cakmak, and M. Boga, "Anticholinesterase and antioxidant activities of novel heterocyclic schiff base derivatives containing an aryl sulfonate moiety," *J. Chin. Chem. Soc.*, vol. 69, pp. 731–743, 2022. DOI: 10.1002/jccs.202100511.

[16] D. Shobha and S. Borhade, "Synthesis, structure, spectroscopy and antimicrobial activity of copper (ii) complex of furfuraldehyde-2-salisaldehyde thiosemicarbazide," *Int. J. Recent Trends Sci. Technol.*, vol. 10, no. 3, pp. 423–429, 2014, Available online.

[17] M. M. E. Shakdofa, A. N. Al-Hakimi, F. A. Elsaied, et al., "Synthesis, characterization and bioactivity of zn2+, cu2+, ni2+, co2+, mn2+, fe3+, ru3+, vo2+ and uo2(2+) complexes of 2-hydroxy-5-((4-nitrophenyl)diazenyl)benzylidene-2-(p-tolylamino)acetohydrazide," *Bull. Chem. Soc. Ethiop.*, vol. 31, no. 1, pp. 75–91, 2017. DOI: 10.4314/bcse.v31i1.7.

[18] H. Ericsson, G. Tunevall, and K. Wickman, "The paper disc method for determination of bacterial sensitivity to antibiotics: Relationship between the diameter of the zone of inhibition and the minimum inhibitory concentration," *Scand. J. Clin. Lab. Investig.*, vol. 12, no. 4, pp. 414–422, 1960. DOI: 10.3109/00365516009065406.

[19] A. M. Ajlouni, Z. A. Taha, W. AlMomani, and A. K. Hijazi, "Synthesis, characterization, biological activities, and luminescent properties of lanthanide complexes with n,n′-bis(2-hydroxy-1-naphthylidene)-1,6-hexadiimine," *Inorganica Chimica Acta*, vol. 388, pp. 120–126, 2012. DOI: 10.1016/j.ica.2012.03.029.

[20] E. M. Abdalla and M. Abd-Allah, "Synthesis, characterization, antimicrobial and antitumor activity of binary and ternary neodymium (iii) complex with 2,2′-((1e,1′e)-(ethane-1,2-diylbis(azaneylylidene))bis(methaneylylidene))diphenol and imidazole," *Egypt. J. Chem.*, vol. 65, no. SI:13, pp. 735–744, 2022. DOI: 10.21608/ejchem.2022.179421.7282.

[21] M. S. A. Galil, A. N. Al-Hakimi, R. Y. Alshwafy, R. A. A. Okab, and A. Mutir, "Synthesis, structural studies and microbial evaluation of cu(ii), mn(ii), ni(ii), zn(ii), fe(iii), ru(iii), vo(ii), uo_2(ii) complexes of tetradentate oxime-hydrazon ligand," *Chem. J.*, vol. 1, no. 3, pp. 95–102, 2015.

[22] A. M. Abu-Dief et al., "Synthesis and characterization of new cr(iii), fe(iii) and cu(ii) complexes incorporating multi-substituted aryl imidazole ligand: Structural, dft, dna binding, and biological implications," *Spectrochimica Acta Part A: Mol. Biomol. Spectrosc.*, vol. 228, p. 117 700, 2020. DOI: 10.1016/j.saa.2019.117700.

[23] S. K. Yassin, J. M. Alshawi, and Z. A. Salih, "Synthesis, characterization and cytotoxic activity study of cu(ii), co(ii), mn(ii), ni(ii) and cr(iii) metal complexes with new guanidine schiff base against hepatocellular carcinoma (hcam) cancer cell," *Egypt. J. Chem.*, vol. 63, no. 10, pp. 4005–4016, 2020. DOI: 10.21608/ejchem.2020.37893.2778.

[24] N. N. Al-Mohammed and T. A. Abdullah, "Antimicrobial activity of transition metal complexes: Structure activity relationships," *Appl. Microbiol.*, vol. 3, no. 2, pp. 234–251, 2023. DOI: 10.3390/applmicrobiol3020017.

[25] F. M. Al-Azab, Y. M. S. Jamil, and A. A. M. Al-Gaadbi, "Synthesis and spectroscopic methods on the complexation of co(ii), ni(ii) and cu(ii) with 2-(((1h-indol-3-yl)methylene)amino)acetohydrazide hydrate," *Sana'a Univ. J. Appl. Sci. Technol.*, vol. 1, no. 1, pp. 117–133, 2023. DOI: 10.59628/jast.v1i1.131.

[26] M. S. Hossain, F. K. Camellia, N. Uddin, M. Kudrat-E-Zahan, L. A. Banu, and M. M. Haque, "Synthesis, characterization and antimicrobial activity of metal complexes of n-(4-methoxybenzylidene) isonicotinohydrazone schiff base," *Asian J. Chem. Sci.*, vol. 6, no. 1, 2019. DOI: 10.9734/ajocs/2019/v6i118987.

[27] A. N. El-Khazandar, "Organo-phosphorus schiff bases part (iv): Synthesis and characteristics of some phosphate schiff-base complexes," *Phosphorus, Sulfur, Silicon Relat. Elem.*, vol. 126, no. 1, pp. 243–255, 1997. DOI: 10.1080/10426509708043564.

[28] A. Gupta and R. Sharma, "Phosphoryl-containing schiff bases as versatile ligands for metal ion coordination," *Inorg. Chem. Front.*, vol. 9, no. 4, pp. 789–802, 2022. DOI: 10.1039/D1QI01322F.

[29] M. N. Uddin et al., "Spectral and computational chemistry studies for the optimization of geometry of dioxomolybdenum (vi) complexes of some unsymmetrical schiff bases as antimicrobial agent," *J. Coord. Chem.*, vol. 71, no. 23, pp. 3874–3892, 2018. DOI: 10.1080/00958972.2018.1533125.

[30] A. K. Singh and R. Singh, "Recent advances in schiff base metal complexes as antimicrobial agents," *Coord. Chem. Rev.*, vol. 441, p. 213 981, 2021. DOI: 10.1016/j.ccr.2021.213981.

[31] A. P. Mishra et al., "Biological applications of schiff base and its metal complexes: A review," *J. Mol. Struct.*, vol. 1250, p. 131 751, 2022. DOI: 10.1016/j.molstruc.2021.131751.

[32] M. A. Mahmood et al., "Structure–activity relationship of schiff bases: Influence of substituents on antimicrobial properties," *J. Saudi Chem. Soc.*, vol. 23, no. 5, pp. 568–580, 2019. DOI: 10.1016/j.jscs.2019.01.006.

[33] S. A. Khan et al., "Antimicrobial behavior of organophosphorus derivatives and their metal complexes," *J. Organomet. Chem.*, vol. 953, p. 122 061, 2021. DOI: 10.1016/j.jorganchem.2021.122061.

[34] M. Patel et al., "Mechanisms of antibacterial action of schiff bases and their complexes: Insights from biochemical assays," *Microb. Pathog.*, vol. 178, p. 106 089, 2023. DOI: 10.1016/j.micpath.2023.106089.

[35] S. Li et al., "Metal–schiff base complexes as emerging antimicrobial agents: A comprehensive review," *J. Inorg. Biochem.*, vol. 213, p. 111 279, 2020. DOI: 10.1016/j.jinorgbio.2020.111279.